Mathematical Biosciences and Engineering

MBE, 19(1): 102–114.
DOI: 10.3934/mbe.2022005
Received: 31 July 2021
Accepted: 27 October 2021
Published: 8 November 2021

http://www.aimspress.com/journal/MBE

Research article

Recognition study of denatured biological tissues based on multi-scale rescaled range permutation entropy

Bei Liu[1,*], Wenbin Tan[1], Xian Zhang[2], Ziqi Peng[1] and Jing Cao[1]

[1] College of Mathematics and Physics, Hunan University of Arts and Science, Changde 415000, China

[2] Key Laboratory of Metallogenic Prediction of Nonferrous Metals and Geological Environment, Monitoring Ministry of Education, School of Geosciences and Info-Physics, Central South University, Changsha 410083, China

* **Correspondence:** Email: liubei@huas.edu.cn.

Abstract: The recognition of denatured biological tissue is an indispensable part in the process of high intensity focused ultrasound treatment. As a nonlinear method, multi-scale permutation entropy (MPE) is widely used in the recognition of denatured biological tissue. However, the traditional MPE method neglects the amplitude information when calculating the time series complexity. The disadvantage will affect the recognition effect of denatured tissues. In order to solve the above problems, the method of multi-scale rescaled range permutation entropy (MRRPE) is proposed in this paper. The simulation results show that the MRRPE not only includes the amplitude information of the signal when calculating the signal complexity, but also extracts the extreme volatility characteristics of the signal effectively. The proposed method is applied to the HIFU echo signals during HIFU treatment, and the support vector machine (SVM) is used for recognition. The results show that compared with MPE and the multi-scale weighted permutation entropy (MWPE), the recognition rate of denatured biological tissue based on the MRRPE is higher, up to 96.57%, which can better recognize the non-denatured biological tissues and the denatured biological tissues.

Keywords: HIFU; multi-scale rescaled range permutation entropy; biological tissue; denatured recognition

1. Introduction

Nowadays, high intensity focused ultrasound (HIFU) has been widely used in tumor treatment [1–3]. HIFU has the advantages of non-invasiveness and safety compared with traditional tumor therapy (surgical resection, chemotherapy and radiotherapy) [4]. HIFU treatment is focused on the tumor target area by high intensity ultrasound, so that the target temperature rises rapidly. When the target temperature exceeds 63 °C, the protein of the lesion tissue in the target location becomes denatured, and does not destroy the normal tissues and cells outside the target area, so as to destroy the cancer cells [5–7]. Therefore, in the process of HIFU treatment, it is the key to ensure the safety and efficiency of HIFU treatment to accurately detect whether the biological tissue in the target area has been denatured [8,9].

So far, HIFU researchers generally employ ultrasound technology to monitor the whole treatment process of HIFU [10–12]. Ralf Seip et al. used the energy characteristics of ultrasonic echo signals to detect whether denatured biological tissue occurred during HIFU treatment. The experimental results showed that the denatured recognition accuracy based on signal energy characteristics reached 82% [13]. In reference [14], the sound velocity characteristics of ultrasonic echo signals were used to monitor the biological tissues during HIFU treatment, and the results showed that the sound velocity of denatured biological tissues was higher than that of non-denatured tissues. However, the sound velocity measurement of biological tissue is easily affected by environmental noise, resulting in inaccurate identification results of denatured biological tissue. From a non-linear perspective, HIFU treatment will change the entropy value of ultrasonic echo signals in biological tissues [15–17]. Bandt et al. [18] proposed the multi-scale permutation entropy (MPE) method. MPE has the advantages of simple calculation and strong anti-noise ability [19–21]. In reference [22], MPE, as the feature of the ultrasonic echo signals, was used to distinguish the non-denatured biological tissue and the denatured biological tissue during HIFU treatment. However, MPE does not contain amplitude information of time series, which reduces the recognition effect for ultrasonic echo signals [23–25]. The multi-scale weighted permutation entropy (MWPE) was proposed to improve the inherent defect of MPE, which includes the amplitude information of time series [26]. In reference [27], MWPE was employed for the recognition of denatured biological tissue during HIFU treatment. However, MWPE adopts the variance as weight still experiences major limitations in terms of analyses of nonlinear signals with extreme volatility. For example, the MWPE method cannot extract the extreme volatility characteristics of the signal effectively when calculating the time series complexity, which will affect the recognition effect. In reference [28], the rescaled range permutation entropy (RRPE) was proposed to extract the characteristics of extreme volatility. In view of the above problems, the recognition method of denatured biological tissue based on multi-scale rescaled range permutation entropy (MRRPE) is proposed in this paper. Compared with MPE and MWPE, MRRPE selects the ratio of range and standard deviation as the weight of different fragments in the time series, thereby including the amplitude information of time series and effectively extracting the extreme volatility characteristics, which improves the resolution and separability of entropy.

In this paper, The MRRPE method is applied to the HIFU echo signals during HIFU treatment, and then the support vector machine (SVM) is used to realize the recognition of denatured biological tissue during HIFU treatment. In addition, the optimal embedding dimension and scale factor parameters of the MRRPE method are discussed, and compared with MPE and MWPE methods, the advantages of the MRRPE methods are illustrated.

2. Principles and methods

2.1. Multi-scale permutation entropy

Multi-scale permutation entropy combines coarse-grained processing with permutation entropy algorithm, which can effectively extract nonlinear features of time series. The calculation steps are as follows:

1) For time series $X = \{x_1, x_2, \ldots, x_N\}$, it can be reconstructed in phase space as follows:

$$X^{m,\tau} = \left\{X^{m,\tau}(1), X^{m,\tau}(2), \ldots, X^{m,\tau}(k) \ldots, X^{m,\tau}(N - (m-1)\tau)\right\} \tag{1}$$

where m is embedding dimension , τ is delay time, $X^{m,\tau}(k)$ can be defined as:

$$X^{m,\tau}(k) = \{x(k), x(k+\tau), \ldots, x(k+(m-1)\tau)\} \tag{2}$$

where $k = 1,2,\ldots, N - (m-1)\tau$.

2) The time reconstruction sequence $\{x(k), x(k+\tau), \ldots, x(k+(m-1)\tau)\}$ is arranged in ascending order. The symbol sequence can be obtained as $\{x(k+(v_1-1)\tau) \le x(k+(v_2-1)\tau) \le \cdots \le x(k+(v_m-1)\tau)\}$. Where $\pi_l^{m,\tau}$ has $m!$ possible values, $\pi_l^{m,\tau}$ can be expressed as:

$$\pi_l^{m,\tau} = \{v_1, v_2, \cdots, v_m\} \tag{3}$$

3) $p(\pi_l^{m,\tau})$ is defined as:

$$p(\pi_l^{m,\tau}) = \frac{\left\|\left\{k \mid k = 1,\ldots, N-(m-1)\tau; X_l^{m,\tau} has\, \pi_l^{m,\tau}\, type\right\}\right\|}{N - (\mathrm{m}-1)\tau} \tag{4}$$

4) Permutation entropy (PE) [18] can be defined as:

$$PE(X, m, \tau) = -\sum_{l:\pi_l^{m,\tau} \in \Pi} p(\pi_l^{m,\tau}) \ln\left(p(\pi_l^{m,\tau})\right) \tag{5}$$

5) The time series $X = \{x_1, x_2, \ldots, x_N\}$ with the length of N is coarse-grained. The coarse- grained sequences $y^s(j)$ are obtained by the Eq (6).

$$y^s(j) = \frac{1}{s} \sum_{i=(j-1)s+1}^{js} x(i) \tag{6}$$

where $j = 1,2,\ldots,[N/s]$. s represents scale factor.

6) The multi-scale permutation entropy (MPE) is defined as:

$$MPE(X, m, \tau, s) = PE(y^s, m, \tau) \tag{7}$$

2.2. Multi-scale weighted permutation entropy

MPE does not contain amplitude information of time series, which reduces the recognition effect. In order to solve the problem, multi-scale weighted permutation entropy (MWPE) was proposed based on MPE method. The calculation steps are as follows:

1) According to the definition of permutation entropy $PE(X,m,\tau)$ in the Eq (5), $p(\pi_l^{m,\tau})$ is weighted , so $p_\omega(\pi_l^{m,\tau})$ can be obtained by the Eq (5).

$$p_\omega(\pi_l^{m,\tau}) = \frac{\left\| \{k \mid k = 1,\ldots,N-(m-1)\tau; X_l^{m,\tau} has\, \pi_l^{m,\tau}\, type\} \right\| \omega_k}{\{N-(m-1)\tau\}\omega_k} \tag{8}$$

where ω_k is expressed as:

$$\omega_k = \frac{1}{m}\sum_{q=1}^{m}\left[x(k+(q-1)\tau) - \overline{X}^{m,\tau}(k)\right]^2 \tag{9}$$

where $\overline{X}^{m,\tau}(k) = \frac{1}{m}\sum_{q=1}^{m}[x(k+(q-1)\tau)]$.

According to Eqs (5) and (8), the weighted permutation entropy $WPE(X,m,\tau)$ [26] is defined as:

$$WPE(X,m,\tau) = -\sum_{l:\pi_l^{m,\tau}\in\Pi} p_\omega(\pi_l^{m,\tau})\ln(p_\omega(\pi_l^{m,\tau})) \tag{10}$$

2) The multi-scale weighted permutation entropy (MWPE) is defined as:

$$MWPE(X,m,\tau,s) = WPE(y^s,m,\tau) \tag{11}$$

2.3. Multi-scale rescaled range permutation entropy

MWPE includes the amplitude information of time series, but MWPE cannot extract the extreme volatility characteristics of the signal effectively when calculating the time series complexity. Therefore, the multi-scale rescaled range permutation entropy (MRRPE) is proposed by selecting the ratio of range and standard deviation as the weight of different fragments in the time series, which includes the amplitude information of time series and effectively extracts the extreme volatility characteristics. The calculation steps are as follows:

1) According to the definition of the weighted permutation entropy $WPE(X,m,\tau)$ in the Eqs (9) and (10), the ratio of range and standard deviation is selected as the weight. So ω_k^R is expressed as:

$$\omega_k^R = \frac{Range(X(k))}{Std(X(k))} \tag{12}$$

According to Eqs (10) and (12), the rescaled range permutation entropy $RRPE(X,m,\tau)$ [28] is defined as:

$$RRPE(X,m,\tau) = -\sum_{l:\pi_l^{m,\tau}\in\Pi} p_R(\pi_l^{m,\tau})\ln(p_R(\pi_l^{m,\tau})) \tag{13}$$

where $p_R\left(\pi_l^{m,\tau}\right)=\frac{\left\|\left\{k \mid k=1,\ldots,N-(m-1)\tau; X_l^{m,\tau} has\, \pi_l^{m,\tau}\, type\right\}\right\|\omega_k^R}{\left\{N-(\mathrm{m}-1)\tau\right\}\omega_k^R}$.

2) The multi-scale rescaled range permutation entropy (MRRPE) is defined as:

$$MRRPE\left(X,m,\tau,s\right)=RRPE\left(y^s,m,\tau\right) \tag{14}$$

3. Experimental result and discussion

3.1. Experimental system

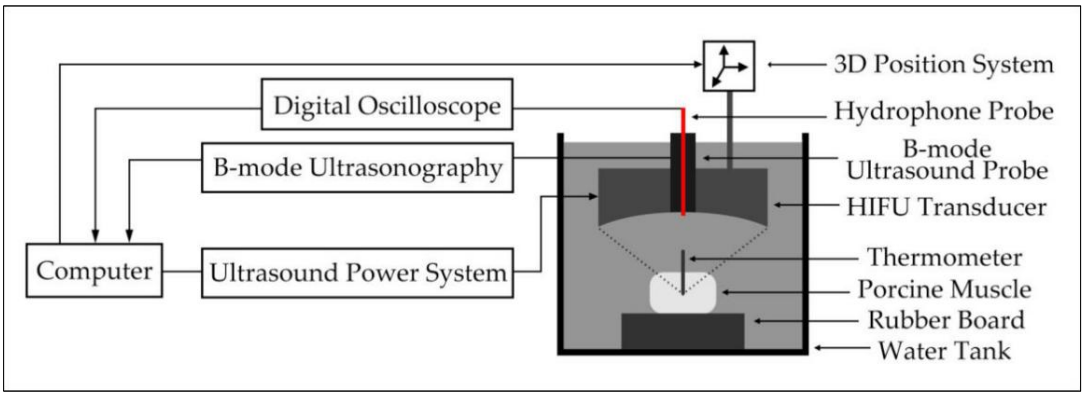

Figure 1. HIFU irradiation experimental system.

(a) (b)

Figure 2. The diagram of non-denatured and denatured tissues slices: (a) Non-denatured tissue; (b) Denatured tissue.

The HIFU irradiation experiment system is shown in Figure 1. Before the irradiation experiment, povidone is added into the water tank to remove the bubbles in the water, so as not to affect the experimental results. Fresh in-vivo porcine muscle tissue is fixed on the rubber plate and placed directly under the HIFU transducer. The HIFU control system is operated by a computer to adjust the irradiation position of the HIFU transducer. The HIFU transducer is employed to irradiate porcine

muscle tissue. The center frequency of the HIFU transducer is 1.39 MHz. The irradiation power of the HIFU transducer is 210–300 W. The HIFU transducer is turned off after irradiation. The B-type ultrasonic probe on the top of the HIFU transducer is used to monitor the HIFU irradiation area, and the fiber-optic hydrophone (FOPH 2000, Germany) is used to receive the HIFU echo signal. Then the digital oscilloscope (Tektronix, MDO3032, USA) is used to average the signal 50 times to improve the signal-to-noise ratio. The received HIFU echo signal is converted into a digital signal by the digital oscilloscope and stored in the computer. In this paper, a total of 292 HIFU echo signals (including 146 non-denatured states and 146 denatured states) are obtained from 15 porcine muscle tissues. In addition, the thermometers at the HIFU irradiation target area are used to measure the temperature of the irradiation area. The denatured state of biological tissue slices is obtained. The diagrams of non-denatured and denatured tissue slices are shown in Figure 2.

3.2. Comparison between different entropies of simulated signals

To further illustrate the advantages of the MRRPE method, according to the published reports [28], the Rössler sequences are generated as the simulated signals. Here, S1, S2, S3, S4, S5 and S6 are the six Rössler sequences with different information structures:

$$\dot{x} = -(y+z); \dot{y} = x + ay; \dot{z} = bx + xz - cz \tag{15}$$

Rössler sequence S1: The parameters of a, b and c are configured as 0.3, 0.4 and 4.5.
Rössler sequence S2: The parameters of a, b and c are configured as 0.29, 0.4 and 3.1.
Rössler sequence S3: The parameters of a, b and c are configured as 0.386, 0.35 and 3.8.
Rössler sequence S4: The parameters of a, b and c are configured as 0.37, 0.45 and 3.
Rössler sequence S5: The parameters of a, b and c are configured as 0.38, 0.3 and 4.5.
Rössler sequence S6: The parameters of a, b and c are configured as 0.3, 0.2 and 2.09.

We select the embedding dimension parameter m = 4, delay time τ = 2. The MPE, MWPE and MRRPE of the six Rössler sequences are calculated respectively. The results of different entropy values of the Rössler signal under scale factors 1–20 are shown in Figure 3. As shown in Figure 3, the entropy value of MPE, MWPE and MRRPE increase with the increase of scale factor. It can be clearly seen that the MPE values curves of six different Rössler sequences have more overlap and poor resolution. Although MWPE has a higher resolution than MPE, the MWPE values curves of the sequences S2 and sequences S3, sequences S5 and sequences S6 still overlap, respectively. Compared with MPE and MWPE, MRRPE values curves of six different Rössler sequences have no overlap. In addition, the resolution between each MRRPE curve of S1, S2, S3, S4, S5 and S6 is more obvious with the increase of scale. This means that MRRPE not only includes the amplitude information of the signal when calculating the signal complexity, but also extracts the extreme volatility characteristics of the signal effectively, which improves the resolution when analyzing the simulated signals.

3.3. Comparison between different entropies of actual HIFU echo signals

As shown in Figures 4 and 5, the time-domain diagram and frequency spectrum of HIFU echo signals of non-denatured tissue and denatured tissue are shown respectively. The number of sampling

points of the HIFU echo signals is 10000. The center frequency of the HIFU echo signals is 1.39 MHz. The MPE, MWPE and MRRPE methods are used to calculate the entropy value of 292 HIFU echo signals (including 146 non-denatured and 146 denatured states). We choose the delay time parameter as 2, the embedding dimension parameter as 4, 5, 6, 7, 8, and the scale factor parameter as 1–15. Support vector machine (SVM) is used to classify and recognize the extracted features. The kernel function of SVM is selected as the radial basis function (RBF). Then, 146 HIFU echo signals (including 73 non-denatured and 73 denatured states) are randomly selected as the training set, and the remaining 146 HIFU echo signals are selected as the test set.

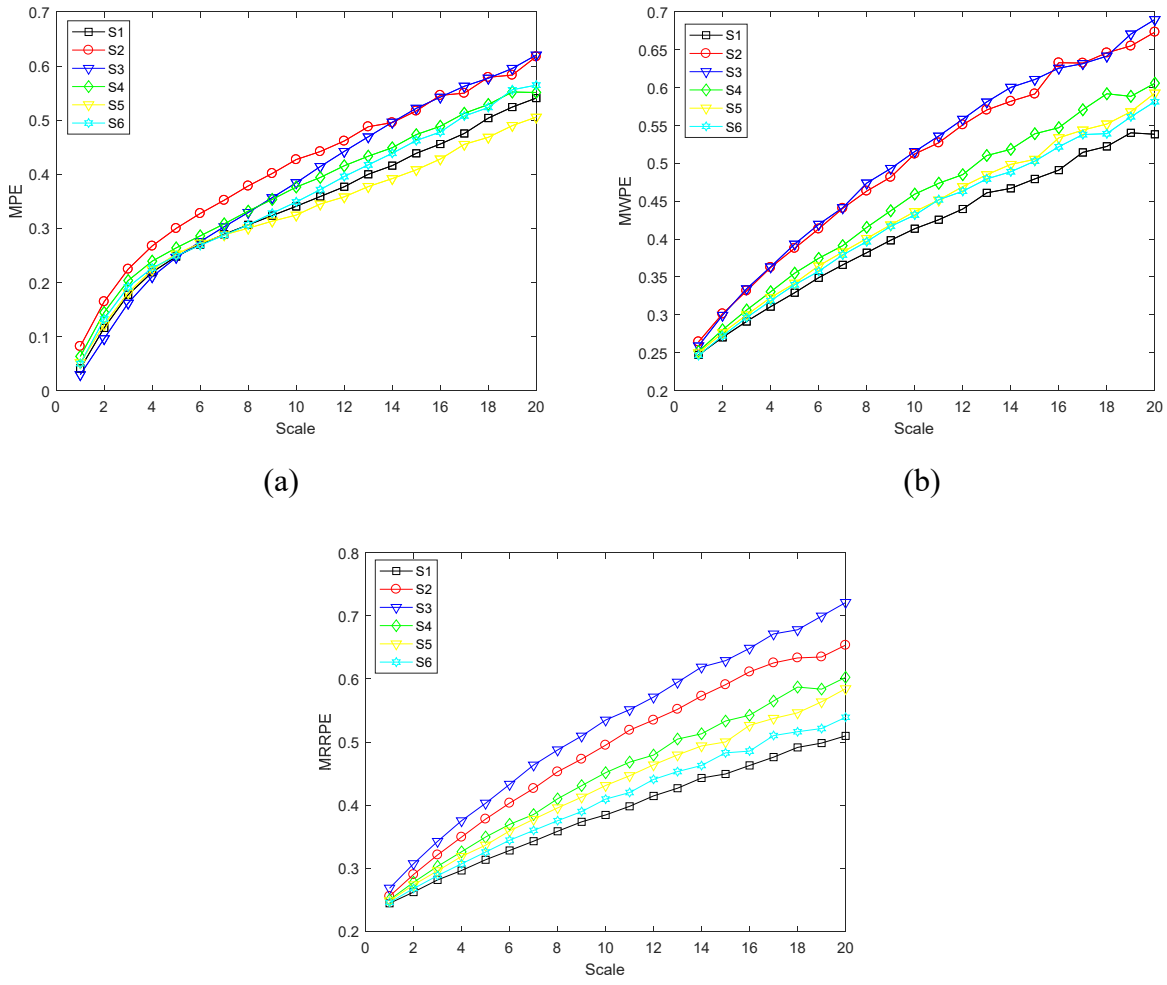

Figure 3. The results of MPE, MWPE and MRRPE of the Rössler signals: (a) MPE; (b) MWPE; (c) MRRPE.

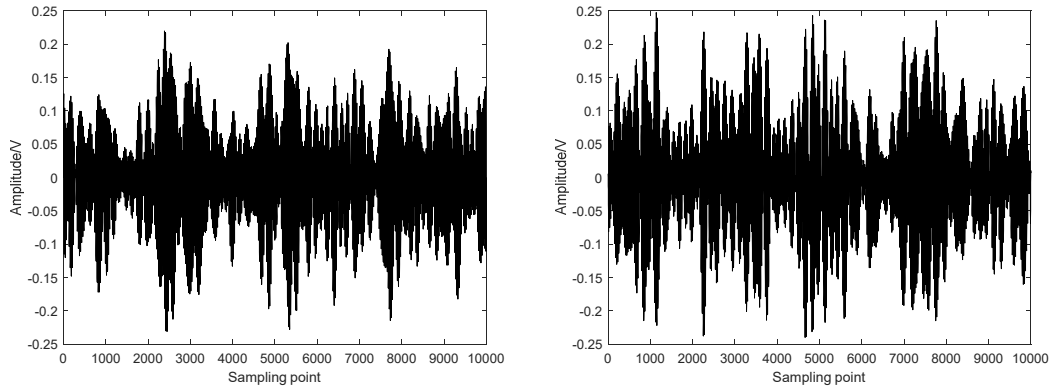

(a) (b)

Figure 4. The HIFU echo signals of non-denatured tissue and denatured tissue: (a) Non-denatured tissue; (b) Denatured tissue.

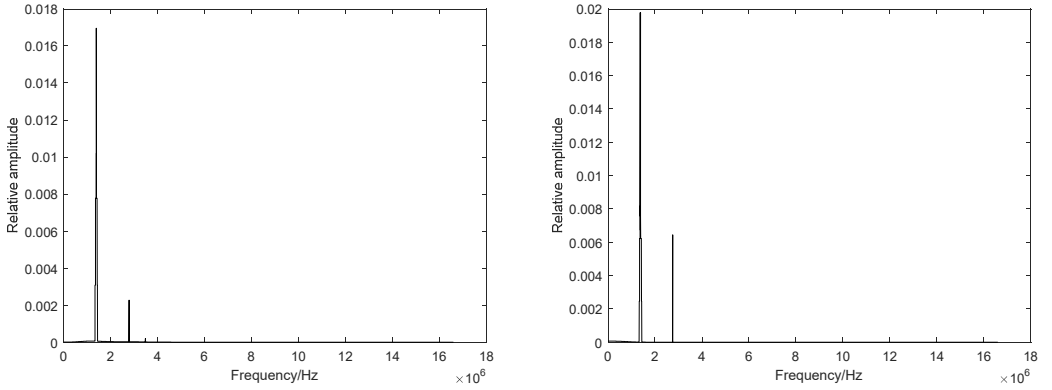

(a) (b)

Figure 5. The frequency spectrum of non-denatured tissue and denatured tissue: (a) Non-denatured tissue; (b) Denatured tissue.

The denatured recognition results of MPE, MWPE and MRRPE features under different embedding dimensions and scale factor parameters are shown as shown in Figure 6. It is clearly seen that when the scale factor parameter is too small (for example, when the scale factor is 1 or 2), the recognition accuracy of denatured biological tissue is low. This is because the advantage of the multi-scale entropy feature analysis method cannot be well reflected due to the small scale factor parameter. Meanwhile, too large scale factor parameter will enhance the entropy fluctuation of each coarse-grained sequence, which will decrease the recognition accuracy. As shown in Figure 6(a), when the embedding dimension is 6 and the scale factor is 13, the recognition accuracy of MPE is the highest. As shown in Figure 6(b), when the embedding dimension is 6 and the scale factor is 13, the MWPE method has the highest recognition accuracy. Compared with MPE and MWPE methods, the recognition accuracy based on MRRPE is higher. In addition, as shown in Figure 6(c), when the embedding dimension is 6 and the scale factor is 14, the recognition accuracy of MRRPE is the highest.

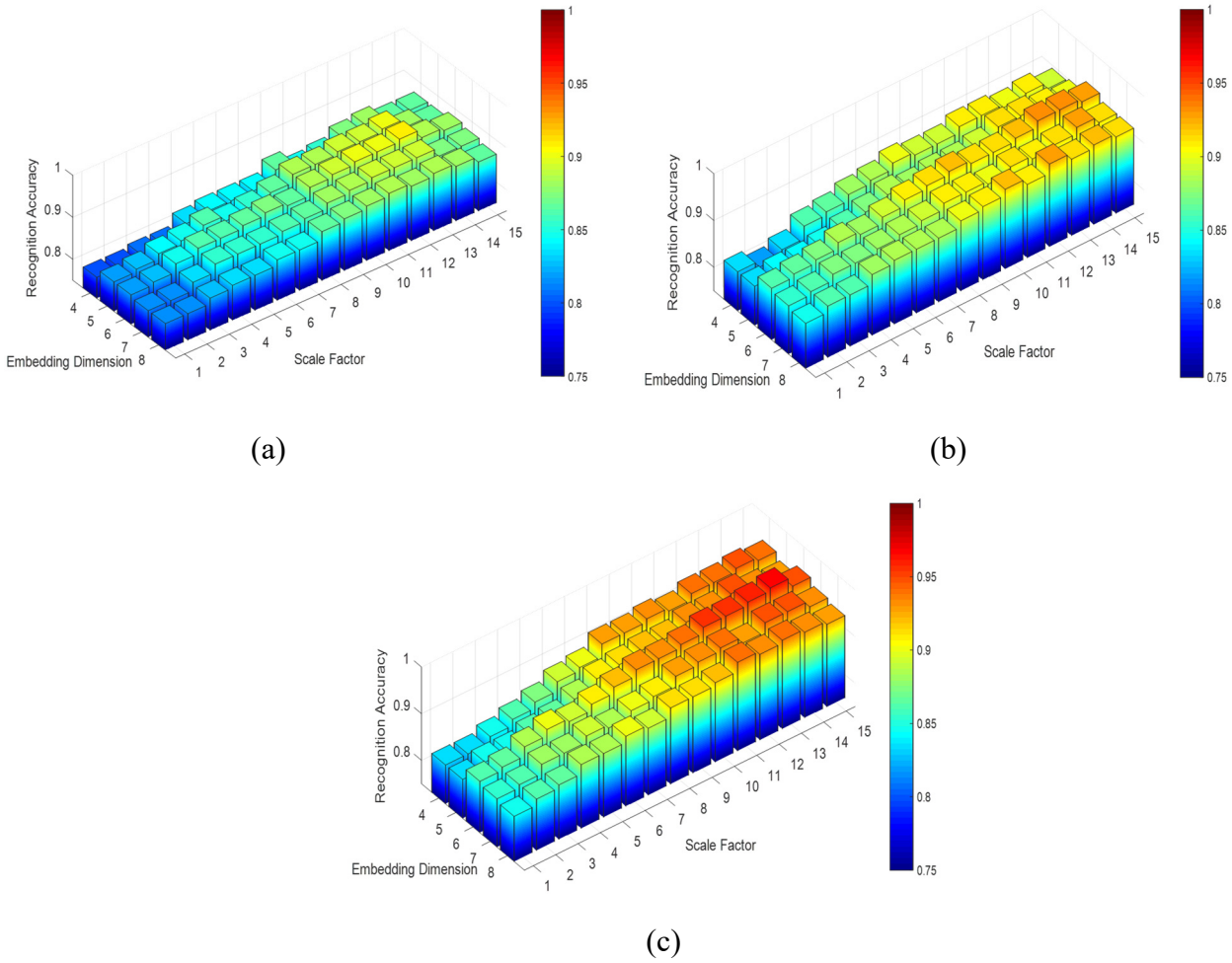

Figure 6. The recognition results of denatured biological tissue based on MPE, MWPE and MRRPE: (a) MPE; (b) MWPE; (c) MRRPE.

To further demonstrate the advantages of the proposed method, the best SVM recognition results of denatured biological tissue based on the MPE, MWPE and MRRPE are compared. Figure 7 shown the SVM recognition diagrams of MPE, MWPE and MRRPE. It can be seen that Abscissa 1 to 73 are non-denatured tissue samples, 74 to 146 are denatured tissue samples. The ordinate type 1 represents the non-denatured tissue status, type 2 represents the denatured tissue status. Compared with MPE and MWPE methods, the MRRPE method has fewer misidentification samples of non-denatured tissues and denatured tissues. The recognition rate of denatured biological tissue based on MRRPE reaches 96.57%, which means that the recognition method of denatured biological tissue based on MRRPE can better identify whether biological tissue has been denatured compared with MPE and MWPE.

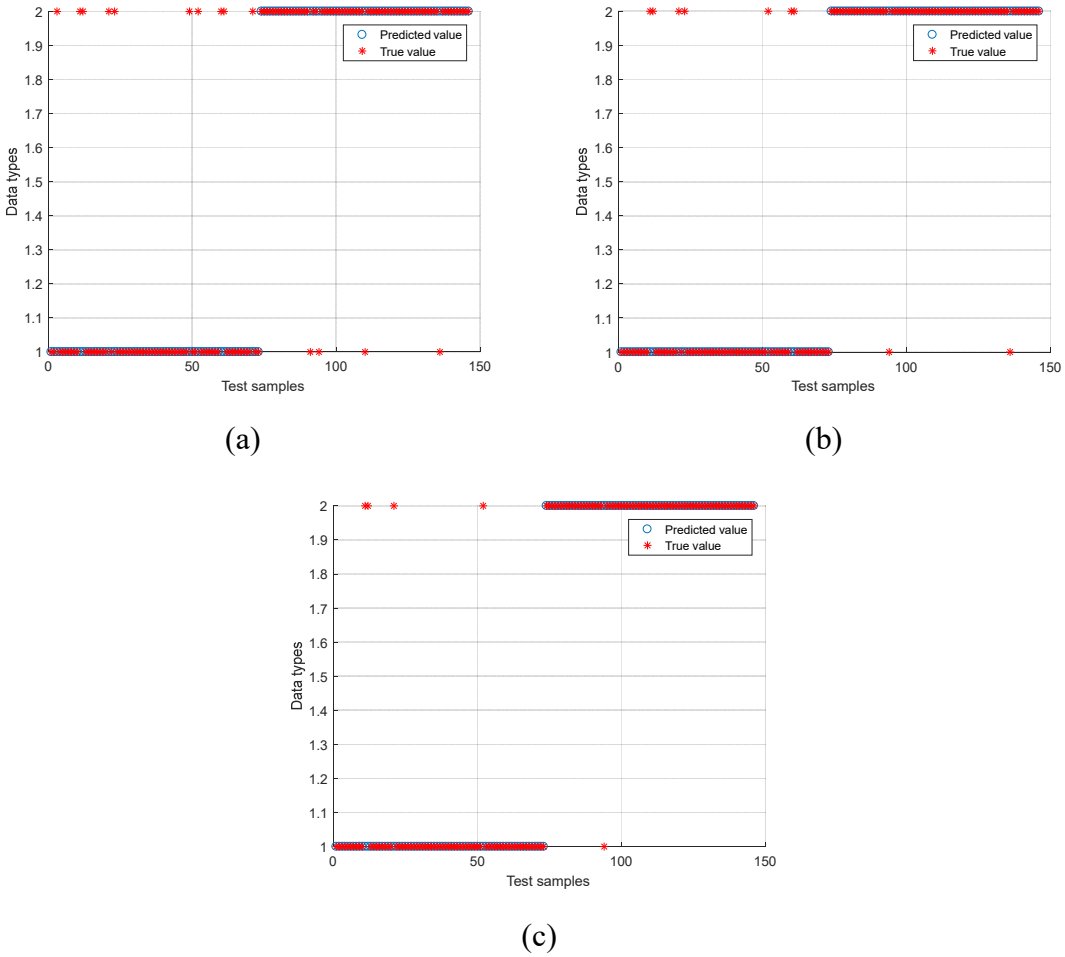

Figure 7. The SVM recognition diagrams based on MPE, MWPE and MRRPE: (a) MPE; (b) MWPE; (c) MRRPE.

4. Conclusions

This paper realizes the identification of denatured tissues based on MRRPE of HIFU echo signals. To solve the shortcoming of the MPE method, the MRRPE method is proposed to improve the resolution. The simulation results show that compared with MPE and MWPE, the MRRPE method not only includes the amplitude information of the signal when calculating the signal complexity, but also extracts the extreme volatility characteristics of the signal effectively. In addition, the proposed method is applied to the actual HIFU echo signals, the results show that the recognition accuracy of MRRPE for the denatured biological tissues is higher than that of MPE and MWPE regardless of embedding dimension of 4, 5, 6, 7 and 8. When the embedding dimension is 6 and the scale factor is 14, the recognition accuracy of MRRPE is the highest, up to 96.57%. The above results demonstrate that compared with MPE and MWPE, the recognition method of denatured biological tissue based on MRRPE can better identify whether biological tissue has been denatured.

However, some parameters in the proposed method need to be set according to manual experience. We consider using the artificial intelligence method to optimize the algorithm parameters in future work.

Acknowledgments

This work was supported by the National Natural Science Foundation of China under grant No. U2031112, the Hunan Provincial Natural Science Foundation of China under grant No. 2020JJ5396, the Excellent Young Scientist Foundation of Hunan Provincial Education Department under grant No. 20B405 and the Research Foundation for Advanced Talents under grant No. E07021011. The authors sincerely thank the anonymous reviewers for their helpful comments and suggestions.

Conflict of interest

The authors declare no conflict of interest in this paper.

References

1. M. Diana, L. Schiraldi, Y. Y. Liu, R. Memeo, D. Mutter, P. Pessaux, et al., High intensity focused ultrasound (HIFU) applied to hepato-bilio-pancreatic and the digestive system-current state of the art and future perspectives, *Hepatobiliary Surg. Nutr.*, **5** (2016), 329. doi: 10.21037/hbsn.2015.11.03.
2. L. Hallez, F.Touyeras, J. Y. KHihn, J. L. Guey, M. Spajer, Y. Bailly, Characterization of HIFU transducers designed for sonochemistry application: Acoustic streaming, *Ultrason. Sonochem.*, **29** (2016), 420–427. doi: 10.1016/j.ultsonch.2015.10.019.
3. M. Marinova, M. Rauch, M. Mücke, High-intensity focused ultrasound (HIFU) for pancreatic carcinoma: evaluation of feasibility, reduction of tumour volume and pain intensity, *Eur. Radiol.*, **26** (2016), 1–10. doi: 10.1007/s00330-016-4239-0.
4. W. Lei, J. Hu, Y. Liu, W. Liu, X. Chen, Numerical evaluation of high-intensity focused ultrasound-induced thermal lesions in atherosclerotic plaques, *Math. Biosci. Eng.*, **18** (2021), 1154–1168. doi: 10.3934/mbe.2021062.
5. D. Cranston, A review of high intensity focused ultrasound in relation to the treatment of renal tumours and other malignancies, *Ultrason. Son.*, **27** (2015), 654–658. doi: 10.1016/j.ultsonch.2015.05.035.
6. N. Ellens, K. Hynynen, Frequency considerations for deep ablation with high-intensity focused ultrasound: A simulation study, *Med. Phys.*, **42** (2015), 4896–4910. doi: 10.1118/1.4927060.
7. R. P. Ramaekers, M. D. Greef, J. M. M. Breugel, C. T. W. Moonen, M. Ries, Increasing the HIFU ablation rate through an MRI-guided sonication strategy using shock waves: Feasibility in the in vivo porcine liver, *Phys. Med. Biol.*, **61** (2016), 1057–1077. doi: 10.1088/0031-9155/61/3/1057.
8. H. Dong, G. Liu, X. Tong, Influence of temperature-dependent acoustic and thermal parameters and nonlinear harmonics on the prediction of thermal lesion under HIFU ablation, *Math. Biosci. Eng.*, **18** (2021), 1340–1351. doi: 10.3934/mbe.2021070.

9. B. Liu, R. Wang, Z. Peng, L. Qin, Identification of denatured biological tissues based on compressed sensing and improved multiscale dispersion entropy during HIFU treatment, *Entropy*, **22** (2020), 944. doi: 10.3390/e22090944.
10. J. S. Lee, T. E. Kim, J. H. Kim, B. J. Park, Unintended pregnancies with term delivery following ultrasound-guided high-intensity focused ultrasound (USgHIFU) ablation of uterine fibroid and adenomyosis, *Clin. Exp. Obstet. Gyn.*, **45** (2018), 842–844. doi: 10.12891/ceog4472.2018.
11. S. Rahimian, J. Tavakkoli, Estimating dynamic changes of tissue attenuation coefficient during high-intensity focused ultrasound treatment, *J. Ther. Ultrasound.*, **1** (2013), 14. doi: 10.1186/2050-5736-1-14.
12. S. Q. Yan, H. Zhang, B. Liu, H. Tang, S. Y. Qian, Identification of denatured and normal biological tissues based on compressed sensing and refined composite multi-scale fuzzy entropy during high intensity focused ultrasound treatment, *Chin. Phys. B*, **30** (2021), 028704. doi: 10.1088/16741056/abcfa7.
13. R. Seip, J. Tavakkoli, R. F. Carlson, A. Wunderlich, N. T. Sanghvi, K. A. Dines, et al., High-intensity focused ultrasound (HIFU) multiple lesion imaging: comparison of detection algorithms for real-time treatment control, in *2002 IEEE Ultrasonics Symposium*, **2** (2002), 1427–1430. doi: 10.1109/ULTSYM.2002.1192564.
14. T. Shishitani, S. Yoshizawa, S. Umemura, Change in acoustic impedance and sound speed of HIFU-exposed chicken breast muscle, in *2010 IEEE International Ultrasonics Symposium*, (2010), 1384–1387. doi: 10.1109/ULTSYM.2010.5935709.
15. S. Mobasheri, H. Behnam, P. Rangraz, Radio frequency ultrasound time series signal analysis to evaluate high-intensity focused ultrasound lesion formation status in tissue. *J. Med. Signals. Sens.*, **6** (2016), 91. doi: 10.4103/2228-7477.181032.
16. P. H. Tsui, Y. L. Wan, Effects of fatty infiltration of the liver on the Shannon entropy of ultrasound backscattered signals, *Entropy*, **18** (2016), 341. doi: 10.3390/e18090341.
17. M. M. Monfared, H. Behnam, P. Rangraz, High-intensity focused ultrasound thermal lesion detection using entropy imaging of ultrasound radio frequency signal time series, *J. Med. Ultrasound.*, **26** (2018), 24. doi: 10.4103/JMU.JMU_3_17.
18. C. Bandt, B. Pompe, Permutation entropy: a natural complexity measure for time series, *Phys. Rev. Lett.*, **88** (2002), 174102. doi: 10.1103/PhysRevLett.88.174102.
19. Y. Gao, F. Villecco, M. Li, W. Song, Multi-scale permutation entropy based on improved LMD and HMM for rolling bearing diagnosis, *Entropy*, **19** (2017), 176. doi: 10.3390/e19040176.
20. W. P. Yao, T. B. Liu, J. F. Dai, J. Wang, Multiscale permutation entropy analysis of electroencephalogram, *Acta. Phys. Sin*, **63** (2014), 078704. doi: 10.7498/aps.63.078704.
21. J. Murillo-Escobar, Y. E. Jaramillo-Munera, D. A. Orrego-Metaute, E. Delgado-Trejos, D. Cuesta-Frau, Muscle fatigue analysis during dynamic contractions based on biomechanical features and Permutation Entropy, *Math. Biosci. Eng.*, **17** (2020), 2592–2615. doi: 10.3934/mbe.2020142.
22. B. Liu, W. P. Hu, X. Zou, Y. J. Ding, S. Y. Qian, Recognition of denatured biological tissue based on variational mode decomposition and multi-scale permutation entropy, *Acta. Phys. Sin*, **68** (2019), 028702. doi: 10.7498/aps.68.20181772.
23. S. D. Wu, C. W. Wu, S. G. Lin, C. C. Wang, K. Y. Lee, Time series analysis using composite multiscale entropy, *Entropy*, **15** (2013), 1069–1084. doi: 10.3390/e15031069.

24. S. D. Wu, C. W. Wu, S. G. Lin, K. Y. Lee, C. K. Peng, Analysis of complex time series using refined composite multiscale entropy, *Phys. Lett. A*, **378** (2014), 1369–1374. doi: 10.1016/j.physleta.2014.03.034.
25. D. Cuesta-Frau, Permutation entropy: Influence of amplitude information on time series classification performance, *Math. Biosci. Eng.*, **16** (2019), 6842–6857. doi: 10.3934/mbe.2019342.
26. B. Fadlallah, B. Chen, A. Keil, J. Principe, Weighted-permutation entropy: A complexity measure for time series incorporating amplitude information, *Phys. Rev. E*, **87** (2013) 022911. doi: 10.1103/PhysRevE.87.022911.
27. B. Liu, S. Qian, W. Hu, Identification of denatured biological tissues based on time-frequency entropy and refined composite multi-scale weighted permutation entropy during HIFU treatment, *Entropy*, **21** (2019), 666. doi: 10.3390/e21070666.
28. J. C. Zhang, W. K.Ren, N. D. Jin, Rescaled range permutation entropy: a method for quantifying the dynamical complexity of extreme volatility in chaotic time series, *Chinese. Phys. Lett.,* **37** (2020), 090501. doi: 10.1088/0256-307X/37/9/090501.

AIMS Press